Water/Hydrocarbon Interfaces: Effect of Hydrocarbon Branching on Single-Molecule Relaxation†

Janamejaya Chowdhary‡ and Branka M. Ladanyi*

Department of Chemistry, Colorado State University, Fort Collins, Colorado 80523-1872

Received: August 28, 2007; In Final Form: January 4, 2008

Water/hydrocarbon interfaces are studied using molecular dynamics simulations in order to understand the effect of hydrocarbon branching on the dynamics of the system at and away from the interface. A recently proposed procedure for studying the intrinsic structure of the interface in such systems is utilized, and dynamics are probed in the usual laboratory frame as well as the intrinsic frame. The use of these two frames of reference leads to insight into the effect of capillary waves at the interface on dynamics. The systems were partitioned into zones with a width of 5 Å, and a number of quantities of dynamical relevance, namely, the residence times, mean squared displacements, the velocity auto correlation functions, and orientational time correlations for molecules of both phases, were calculated in the laboratory and intrinsic frames at and away from the interface. For the aqueous phase, translational motion is found to be (a) diffusive at long times and not anomalous as in proteins or micelles, (b) faster at the interface than in the bulk, and (c) faster upon reduction of the effect of capillary waves. The rotational motion of water is (a) more anisotropic at the interface than in the bulk and (b) dependent on the orientation of the covalent O−H bond with respect to the plane of the interface. The effect of hydrocarbon branching on aqueous dynamics was found to be small, a result similar to the effect on the interfacial water structure. The hydrocarbon phase shows a larger variation for all dynamical probes, a trend consistent with their interfacial structure.

I. Introduction

The presence of an interface perturbs the structural organization as well as the dynamics of water with respect to the bulk. Characterization of these changes is crucial for understanding natural and industrially important phenomena occurring at the aqueous interfaces formed by biological macromolecules,[1−3] lipid bilayers,[4,5] reverse micelles,[6−9] micelles,[10] liquid/liquid[11−13] and liquid/metal[14] interfaces, and nanopores.[15−18] Since these different systems contain varying proportions of the hydrophobic and hydrophilic components in the nonaqueous phase besides having different shapes for the interface, the study of a planar hydrophobic water/hydrocarbon interface should be a particularly useful first step in a systematic understanding of interfacial dynamics.

While aqueous interfaces with organic liquids have been studied in the past,[11] the attention paid specifically to interfacial dynamics of the water and organic phases has been minimal. Mean squared displacements have been calculated to study diffusion in interfaces formed by water with nitrobenzene,[19] *n*-heptane,[20] *n*-nonane,[21] 1,2-dichloroethane,[22] and 2-heptanone[23] interfaces. The orientational time correlation functions have been obtained for nitrobenzene,[19] *n*-nonane,[21] 1,2-dichloroethane,[22] and 2-heptanone.[23] A systematic study of the effect of the hydrocarbon chain length or branching on interfacial dynamics is still not available. In prior work,[24] we have studied the effect of hydrocarbon branching and capillary waves on the structure of water/hydrocarbon interfaces. Here, we present our results for the dynamics of the system at and away from the interface.

Studies of interfacial water in reverse micelles,[9] micelles,[10] and proteins[3] suggest anomalous diffusive behavior for water, with the mean squared displacement showing a subdiffusive behavior ($\langle \Delta r^2(t) \rangle \propto t^{\alpha}$, with $\alpha < 1$) at long times. Such dynamical behavior of water can be interpreted as a random walk on a fractal surface[3,25] formed by the nonaqueous phase or with a distribution of residence times for water molecules at the interface.[3,25] Of course, it is also possible that the observed anomalous behavior is a result of combining the dynamical behavior normal and tangential to the nonaqueous surface.[26] One of the aims of this work is to investigate the type of dynamics observable for both the water and hydrocarbon components forming the interface.

By analogy with translational motion, the existence of different local environments in the interfacial region can lead to orientational time correlation functions (TCFs) that are described better as stretched exponentials[3] or sums of exponentials[5] rather than as a simple exponential decay. Furthermore, some interfaces provide an environment where rotation might be restricted or hindered.[27,28] It would be useful to determine the behavior of orientational relaxation at interfaces of immiscible liquids such as water/hydrocarbon. In the case of the water phase, recent simulation and theoretical studies have shown that orientational relaxation in the bulk liquid does not follow the prediction of a rotational diffusion model but is better represented in terms of an extended jump model in which large-amplitude angular displacements between different hydrogen-bonding configurations are possible.[29] Therefore, another objective in this work is to test if the extended jump model is applicable to reorientation of interfacial water.

For a liquid/liquid interface, in the absence of an external field, the interface does not exhibit translational motion, although by virtue of the breakdown of translational symmetry, capillary waves[30,31] arise at these interfaces. These capillary waves can affect interfacial properties, and examining their role on dynamics is important. Interfacial properties can be described

† Part of the "Attila Szabo Festschrift".

* To whom correspondence should be addressed. E-mail: bl@lamar.colostate.edu.

‡ E-mail: janamej@lamar.colostate.edu.

10.1021/jp0769025 CCC: $40.75
Published on Web 03/07/2008

in terms of an intrinsic part[24,32] (not broadened by capillary waves) and its capillary wave-broadened counterpart (as observed in the laboratory frame). In previous studies of interfacial structure of water/hydrocarbon interfaces, we utilized a procedure for identifying the intrinsic density profiles and concluded that capillary waves broaden the intrinsic density, profile resulting in the density profiles observed in the laboratory frame.[24] One of ours goals in this work is to extend the intrinsic property analysis to dynamics of the system.

This paper is organized as follows. In section II, we summarize the molecular dynamics simulation details. This is followed by a presentation and discussion of our results for the dynamics at and away from the interface for water in section III and the hydrocarbon in section IV. After this, we present a summary of our results and conclusions in section V.

II. Simulation details

The simulation setup and protocol is summarized here, and details can be found elsewhere.[24] Molecular dynamics simulations were carried out using codes developed in our group for the water/hydrocarbon interfaces using five different hydrocarbons categorized into two series: series 1, the *n*-pentane (P), 2-methyl pentane (2MP), and 2,2,4-trimethyl pentane (TMP); and series 2, *n*-octane (O), 2-methyl heptane (2MH), and 2,2,4-trimethyl pentane (TMP). The force fields adopted are SPC/E[33] for water and united atom OPLS for hydrocarbon molecules.[34,35] Electrostatic interactions were handled with Wolf's method[36−39] which is a faster alternative to the usual Ewald summation[40,41] and leads to the similar dynamics for our interfacial system.[42] Temperature and pressure were kept constant at 298.15 K and 1 atm using Berendsen's thermostat and barostat[43] with coupling times of 20 ps.

The number of water (W) molecules is kept fixed at 586, and the water layer is sandwiched between two hydrocarbon (H) layers, each containing an equal number of molecules. The number of hydrocarbon molecules in each layer was 91 for *n*-pentane, 79 for 2-methyl pentane, and 64 for all other hydrocarbons. This ensures an equal area of the cross section of the interface for all systems. After an initial equilibration run of 250 ps, simulations were continued for an additional 1 ns, and 50 000 configurations were saved at intervals of 20 fs.

The standard tools for interrogating single-molecule relaxation such as the survival time correlation function, waiting time distribution, probability distribution of displacement in a given time, mean squared displacement, velocity autocorrelation, and orientational time correlation functions were used in the analysis of dynamics.[3]

Dynamics were studied in two frames of reference. For the typically used laboratory frame, for each W/H interface, the two liquid phases were partitioned along the z axis into six zones with a width of 5 Å, as illustrated in Figure 1a. For water, we identify the region $-5 < z < 5$ Å as the bulk, the region $z \leq -10$ Å and $z \geq 10$ Å as interfacial, and the remaining water is labeled intermediate. The hydrocarbon phase was likewise partitioned into six zones on either side of the water phase with $-7.5 < z \leq -2.5$ Å and $2.5 \leq z < 7.5$ Å labeled as interfacial, the region $z \leq -32.5$ Å and $z \geq 32.5$ Å labeled as the bulk, and the remaining water is treated as an intermediate (I1, I2, I3, ...), with variation from interfacial to bulk water in the intermediate region (illustrated in Figure 1b). Since a molecule can enter and leave a given zone, different dynamical quantities were calculated for each molecule while it populated a given zone and averaged over all molecules in the zone. Due to the symmetry of the system, all dynamical quantities were averaged over bulk, intermediate, and interfacial regions on either side of the origin of the reference frame before reporting them.

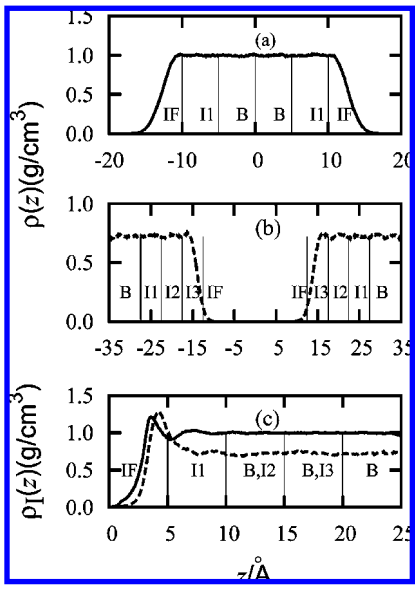

Figure 1. Density profiles and partitioning into different zones illustrated for the water/TMP system; (a) water (solid line), (b) hydrocarbon (dashed line), (c) intrinsic profiles for water with respect to the hydrocarbon surface (solid line) and for the hydrocarbon with respect to the water surface (dashed line). The different regions in the water and hydrocarbon phases are labeled as B (bulk), IF (interfacial) and I1, I2, I3, ... (intermediate). A pair of labels, such as (B,I1), indicates bulk (B) water and intermediate (I1) hydrocarbon zones.

In order to identify the effect of capillary waves at the interface on dynamics of molecules near the interface, the W and H surface sites were identified using a procedure presented elsewhere.[24] The position of the center of mass of the hydrocarbon molecule and oxygen atom of water with respect to the closest water and hydrocarbon surface site, respectively, was calculated, and each liquid phase was partitioned into three (for water) and six (for hydrocarbon) zones of width 5 Å with respect to the surface sites of the other liquid phase (illustrated in Figure 1c). This procedure was used to study the dynamics of each liquid in the "intrinsic frame" as a function of distance from the surface and is a route to minimizing the effect of capillary waves at the interface on dynamics.

III. Water Dynamics

A. Residence Time. The residence time distribution, $w(t)$, provides information about the dynamical behavior of the system. Temporal disorder due to varying interactions of water with the hydrocarbon phase can lead to a residence time distribution with a power law tail ($w(t) \propto t^{\mu}$). Such a distribution of residence times can give rise to anomalous diffusion, as observed in hydration water of proteins and micelles. An exponential decay ($w(t) \propto \exp(-bt)$) would be associated with a Markovian random walk description of dynamics, whereas a stretched exponential distribution (eq 1) can be obtained by having a distribution of residence times about a characteristic value. It is therefore important to quantify the long time tail of the residence time distribution.

For each molecule i in a given zone j at time $t = 0$, we identify the time $\tau_{i,j}$ for which it stays in zone j. Since each molecule can exit and enter the different zones at different stages of the simulation, the distribution of residence times is constructed based on all molecules in zone j, and one obtains the mean residence time as an average of all values of $\tau_{i,j}$ for

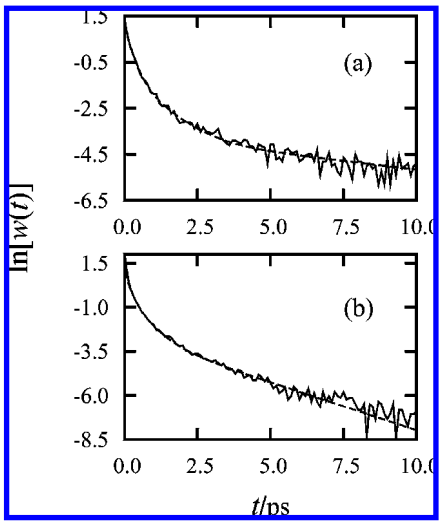

Figure 2. Residence time distribution, $w(t)$, for interfacial water (solid line) in the (a) laboratory frame and (b) intrinsic frame. Also shown is the curve (dashed line) obtained by fitting the data to eq 1.

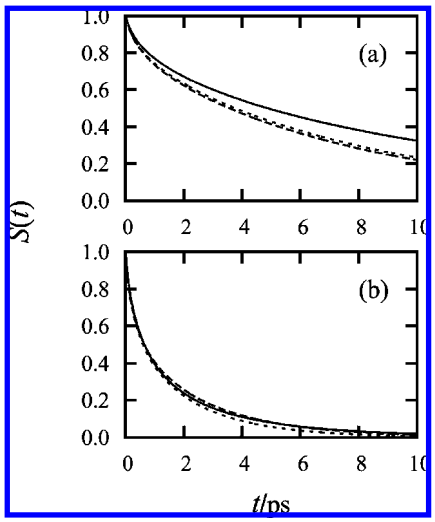

Figure 3. Survival time correlation function for the (a) laboratory frame and (b) intrinsic frame. The different line styles represent interfacial (solid line), intermediate (small dashes), and bulk (large dashes) regions.

all molecules in zone j. We present the residence time distribution for the interfacial region in the laboratory and intrinsic frames in Figure 2a and b, respectively.

For each zone and in both reference frames, the distribution shows a rapid short time decay followed by a long time tail. This initial decay presumably arises due to the short time transient and librational motion that moves a molecule out of the region. The longer time decay could then have a diffusive origin and might be more representative of water in the hydration layer of the hydrocarbon phase. The distribution for $t > 0.25$ ps is fit to a sum of two stretched exponentials, sum of three exponentials, and a power law decay for all distributions and in both frames of reference. On the basis of the root mean squared residual obtained from the fit as well as visual inspection, we find that the sum of stretched exponentials describes the entire time range well. The sum of exponentials is comparable but slightly inferior to the sum of stretched exponentials. The power law decay does not fit the intrinsic frame data but models the laboratory frame data well, although the sum of residuals is the worst among the three functional forms selected. We therefore select the sum of stretched exponentials, eq 1, to model the distribution of residence times and consequently expect diffusive dynamics for our systems

$$w(t) = a_1 \exp[-(t/\tau_1)^{\gamma_1}] + a_2 \exp[-(t/\tau_2)^{\gamma_2}] \qquad (1)$$

To further quantify the residence times in each region, we construct the survival time correlation function, $S(t)$, which corresponds to the probability that a molecule stays in a given zone at time t without exiting the zone for each aqueous region in the laboratory and intrinsic frames. It describes the relaxation of the selected water shells adjacent to the hydrocarbon phase. If $\varsigma(t,t+\tau)$ is the set of molecules that populate a given zone in the time interval $\{t,t+\tau\}$, and if $N(t,t+\tau)$ is the number of molecules in set $\varsigma(t,t+\tau)$ and $N(t)$ is the number of molecules in a given zone at time t, then $S(t)$ can be calculated as

$$S(\tau) = \frac{1}{n_t}\sum_{n=0}^{n_t}\frac{N(n\Delta t, n\Delta t+\tau)}{N(n\Delta t)} \qquad (2)$$

where n_t is the number of time origins considered in the calculation and Δt is the time interval between successive saved MD trajectory data points.

The calculated $S(t)$ are shown in Figure 3 for the water/TMP interface in the laboratory and intrinsic frames. For both frames of reference, $S(t)$ shows a short time decay followed by a slower long time decay. The short time decay can be interpreted in the same way as the waiting distribution and gets contribution from molecules near the boundary of each region that move out of a zone due to small displacements. The longer time decay is more representative of relaxation of the hydration shells adjacent to the interface. Water in the bulk phase shows an almost exponential long time decay and a stretched exponential short time decay. It can also be seen that water nearest to the hydrocarbon phase relaxes slower than that in the bulk phase. The intermediate phase appears to relax slightly slower than the bulk in the laboratory frame.

The time dependence of $S(t)$ in the intrinsic frame is qualitatively similar to that in the laboratory frame. The dynamics is faster than that in the laboratory frame for all regions. Unlike the laboratory frame, intermediate water in the intrinsic frame exhibits a faster relaxation than the interfacial and bulk water. In our study of the intrinsic structure,[24] the average density of the intermediate region, ~ 0.98 g/cm^3, was smaller than that of the bulk, and this could lead to faster relaxation than the bulk. Furthermore, since the definition of interfacial water in the intrinsic frame is based on the distance from the hydrocarbon surface, the motion of water molecules in the intrinsic frame gets an additional contribution from the rearrangement of the hydrocarbon surface and due to capillary waves. Relaxation of the survival time correlation function is therefore expected to be faster in the intrinsic frame compared to that in the laboratory frame for all regions. As a result, $S(t)$ in the bulk phase for lab and intrinsic frames will be different.

We find that the overall shape of $S(t)$ can be best fit to a sum of stretched exponentials over the entire time range and is given by

$$S(t) = a_s \exp[-(t/\tau_s)^{\gamma_s}] + a_1 \exp[-(t/\tau_1)^{\gamma_1}] \qquad (3)$$

where the subscripts s and l correspond to the short and long time components of $S(t)$. The parameters obtained from fits to our simulation data are summarized in Table 1. Since the bulk-phase form of $S(t)$ is almost identical for all interfacial systems studied, we present the fit parameters for the bulk phase of water/TMP and parameters for interfacial water.

TABLE 1: Parameters for the Fit of the Survival Time Correlation Function for Interfacial Water of All Five Water/Hydrocarbon Interfacial Systems to Eq 3[a]

	lab frame						intrinsic frame					
hydrocarbon	a_s	τ_s (ps)	γ_s	a_l	τ_l	γ_l	a_s	τ_s (ps)	γ_s	a_l	τ_l	γ_l
P	0.13	0.44	0.72	0.89	9.94	0.76	0.81	0.59	0.68	0.27	3.33	0.96
2MP	0.14	0.45	0.72	0.88	9.73	0.78	0.64	0.49	0.69	0.44	2.49	0.83
TMP	0.17	0.53	0.71	0.85	10.83	0.82	0.85	0.68	0.65	0.23	3.97	1.0
	(0.23)	(0.50)	(0.71)	(0.79)	(8.35)	(0.97)	(0.52)	(0.25)	(0.66)	(0.58)	(2)	(0.93)
2MH	0.16	0.50	0.72	0.87	10.36	0.8	0.39	0.38	0.67	0.68	1.76	0.71
O	0.17	0.53	0.71	0.85	10.83	0.82	0.67	0.35	0.62	0.44	2.39	1.0

[a] The numbers in parentheses are for the bulk water phase of water/TMP.

For the laboratory frame, the time scale for the short time decay, τ_s, is on the order of 0.5 ps for bulk and interfacial water. Since τ_s is independent of the proximity to the hydrocarbon surface, it could be characteristic of the size of the region selected and might correspond to vibrational or librational motion of the molecule, which may lead to recrossing of the boundary between adjacent zones, thereby leading to the fast initial decay. The stretched exponent, γ_s, is constant at 0.72 for the short time decay, further suggesting the independence of the short time decay on the hydrocarbon phase. Similar values for τ_s and γ_s were extracted for water within 4 Å of a protein[44] and by refitting the survival time correlation function for free water (not bonded to the surfactant head group) of a SDS micelle[45] to a sum of stretched exponentials. While not conclusive, this observation does raise the possibility that the short time variation of $S(t)$ for water molecules in the interfacial region might be similar in different interfacial systems.

The characteristic time for the long time decay, τ_l, shows a variation larger than that of τ_s between the different interfacial systems studied, with the hydrocarbon having the smaller mass in series 1 exhibiting a faster decay, while for the same mass but a different extent of branching in series 2, τ_l shows an insignificant variation. The exponent γ_l shows a similar variation with a small decrease for the lighter hydrocarbon in series 1 and insignificant change for series 2. Clearly in the laboratory frame, the relaxation of each region appears to be affected by the mass of the molecule, albeit not by a large amount.

The slower relaxation of water in the vicinity of the hydrocarbon phase is a feature observed in the hydration water of proteins, micelles, and bilayers. In those systems, the presence of charged moieties can lead to strong hydrogen formation and consequently longer residence times. For our water/hydrocarbon system, the hydrocarbon phase is electrically neutral, unlike the charged surfaces of, for example, proteins. What then might be the reason for this longer residence time near the hydrocarbon surface? A simple rationalization for this longer lifetime of water molecules near the interface is purely geometrical. Adjacent to an interface, water molecules have to move toward the bulk in order to diffuse away from the interface, whereas in the bulk, the molecules are free to move in any direction. This confinement at the interface can lead to the longer residence times observed in our simulation. Since the interfacial widths for all interfacial systems studied here are on the order of 2.3 Å, the effect of molecules trapped in hydrophobic cavities should not be significant. Additionally, water molecules at the interface are known to participate in a more efficiently hydrogen-bonded network. This too could lead to longer residence times for water molecules in the interfacial region.

Turning to the intrinsic frame, τ_s appears to be slightly larger than the corresponding laboratory frame value for series 1 hydrocarbons but smaller than those for series 2. If the short time decay is a function of the size of the region, it should not be surprising to see a similar magnitude of τ_s in the intrinsic and laboratory frames. The τ_s values are, of course, not the same in the two frames of reference. Perhaps the smaller size of the hydrocarbon molecule in series 1 leads to a more compact arrangement at the surface (as observed in the intrinsic structure), thereby leading to a slightly slower motion of the water molecules. Then, the larger molecule, for example, octane, is likely to move faster and might be associated with faster rearrangement of the adjacent water phase, as observable from τ_s values for series 2.

The long time decay of $S(t)$ does not appear to show any systematic variation in both hydrocarbon series. For series 1, τ_l increases from P to TMP, but 2MP shows a slight decrease. As shown elsewhere,[24] the first peak in the intrinsic density profile of water with respect to the hydrocarbon surface is comparable in height and width for P and 2MP, although 2MP has a slightly sharper peak. A slightly sharper peak is indicative of a narrower region adjacent to the hydrocarbon phase populated by interfacial water molecules, and this could lead to the smaller value of τ_l for 2MP as compared to that for P. For the water/TMP interface, the first peak is broader than that for P, thereby indicating a more diffuse interfacial water phase adjacent to the hydrocarbon, and this is the likely reason for the larger value of τ_l for TMP as compared to that for P. A similar trend is apparent for series 2 hydrocarbons as well.

The effect of capillary waves at the interface is to broaden the intrinsic density profile for water near the hydrocarbon surface. The long time decay in the intrinsic frame is therefore expected to be smaller than that in the laboratory frame, with the difference in time scales likely to be related to the relaxation of the hydrocarbon surface. Relaxation times for the surface at interfaces are unknown for liquid/liquid interfaces, and it would be useful to obtain them from simulations in order to test this possible relation between τ_l in the laboratory and intrinsic frames.

B. Translational Motion. *1. Mean Squared Displacement.* The mean squared displacements along each Cartesian direction are calculated based on

$$\langle \Delta x^2(\tau) \rangle = \frac{1}{n_t} \sum_{n=1}^{n_t} \frac{1}{N(n\Delta t, n\Delta t + \tau)} \sum_{i=1}^{N(n\Delta t, n\Delta t+\tau)} [x_i(n\Delta t + \tau) - x_i(n\Delta t)]^2 \quad (4)$$

where the different quantities are defined in section III.A. The diffusion constant can be obtained from the mean squared displacement by taking the long time (τ') limiting value for D_{xx} of the following equation

$$D_{xx} = \frac{\langle \Delta x^2(\tau') \rangle}{2\tau' S(\tau')} \quad (5)$$

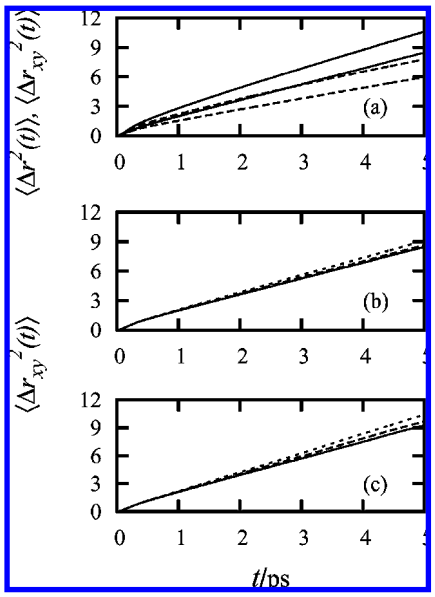

Figure 4. Mean squared displacement (a) for the water/TMP interface from top to bottom at $t = 5$ ps, $\langle \Delta r^2(t) \rangle$ (solid lines), for interfacial and bulk water and the x,y component, $\langle \Delta r_{xy}^2(t) \rangle$ (dashed lines), for interfacial and bulk water, (b) $\langle \Delta r_{xy}^2(t) \rangle$ for interfaces with P (short dashes), 2MP (large dashes), and TMP (solid line) in the laboratory frame, and (c) $\langle \Delta r_{xy}^2(t) \rangle$ for TMP (solid line), 2MP (large dashes), and P (short dashes) in the intrinsic frame.

TABLE 2: In-Plane (D_{xy}) and Out-of-Plane (D_{zz}) Diffusion Constants for the Aqueous Phase of the Five Water/Hydrocarbon Interfacial Systems[a]

	P	2MP	TMP	2MH	O
D_{xy}^{L}	0.45	0.42	0.40	0.41	0.40
D_{xy}^{I}	0.53	0.47	0.45	0.45	0.43
D_{zz}^{L}	0.15	0.15	0.16	0.14	0.13
D_{zz}^{I}	0.14	0.20	0.15	0.15	0.16

[a] Values reported in units of Å^2/ps. Superscripts L and I correspond to laboratory and intrinsic frames. Bulk values are $D_{xy} \approx 0.26$ and $D_{zz} \approx 0.17$.

where $S(\tau)$ is defined in eq 2. This equation is applicable only for the calculation of D_{xx} and D_{yy}.[26] The same expression cannot be used for translational motion in the z direction since the confinement provided by the interface leads to a long time plateau in the mean squared displacement.[26,46−48]

In order to estimate D_{xx} and D_{yy}, data in the time range of 2−5 ps were used. We obtained an approximate value for D_{zz} by calculating the diffusion constant, D, from the total mean squared displacement, $\langle \Delta r^2(t) \rangle = \langle \Delta x^2(t) \rangle + \langle \Delta y^2(t) \rangle + \langle \Delta z^2(t) \rangle$, and the in-plane diffusion constant, D_{xx}, from the mean squared displacement in the (x,y) plane, $\langle \Delta r_{xy}^2(t) \rangle = \langle \Delta x^2(t) \rangle + \langle \Delta y^2(t) \rangle$ (since $D_{xx} \approx D_{yy}$), and using $D_{zz} = 3D - 2D_{xx}$. A more accurate estimate of D_{zz} can be obtained in terms of the analysis of Liu et al.[26]

The mean squared displacement for the x and y directions are similar, and we present the results for the total, $\langle \Delta r^2(t) \rangle$, and in-plane, $\langle \Delta r_{xy}^2(t) \rangle$, in Figure 4a. The time dependence was fit to a power law, $\langle \Delta r^2(t) \rangle \propto t^{\alpha}$, and we obtained a value of α on the order of 0.95−0.98, clearly indicating diffusive behavior at long times. Fits to a linear function were used to extract the values of the diffusion constants, and these are listed in Table 2.

For the laboratory frame, the magnitude and slope of the total mean squared displacement, $\langle \Delta r^2(t) \rangle$, increase from the bulk to interfacial regions, as shown in Figure 4, and this is associated with an increase in $\langle \Delta r_{xy}^2(t) \rangle$. The difference in the magnitude of the total and in-plane mean squared displacement is a small fraction of the total, implying that the mean squared displacement perpendicular to the interface is small, and it consequently gives a smaller diffusion constant in a direction perpendicular to the interface. From Table 2, the diffusion constant for in-plane motion is almost twice as large as the diffusion constant perpendicular to the interfacial plane for all systems. The observed variation in our five systems is consistent with previous studies for water/hydrocarbon interfaces.[20,21]

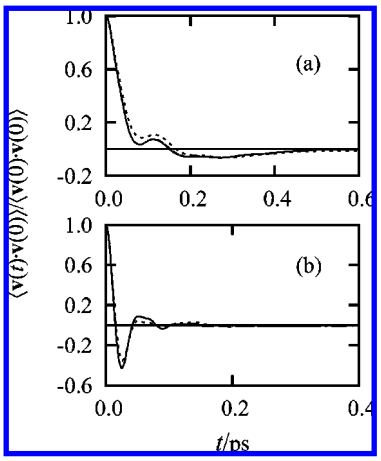

Figure 5. Velocity autocorrelation function for the water/TMP interface in the laboratory frame for the (a) oxygen atom/bulk (solid line) and interfacial water (short dashes) and (b) hydrogen atom/bulk (solid line) and interfacial water (short dashes).

The effect of hydrocarbon branching for series 1 is shown in Figure 4b in the laboratory frame. Going from P to TMP, $\langle \Delta r_{xy}^2(t) \rangle$ shows a slight decrease, suggesting a somewhat faster diffusive motion for water adjacent to the lighter hydrocarbon molecules. For series 2 hydrocarbons, the diffusion constants are comparable, suggesting their independence from the hydrocarbon phase.

In the intrinsic frame, molecular motion should be faster, as already observed in the survival time correlation function. The magnitudes of the in-plane diffusion constants are higher, as expected. Diffusion constants perpendicular to the interface are not significantly changed with respect to the laboratory frame. The intrinsic density profile for water with respect to the hydrocarbon surface shows an enhanced density near it.[24] At constant temperature, an increase in density is a sufficient reason for a decrease in the diffusion constant near the hydrocarbon phase, and this is also apparent in the laboratory frame.

2. *Velocity Autocorrelation Function.* The presence of an interface not only affects diffusive motion but it can also affect the librational motion of water molecules and nondiffusive dynamics of the hydrogen-bonded network. This change due to interactions at the interface can be probed by comparing the shape of the intermolecular vibrational spectrum of the bulk and interfacial phases. To obtain these vibrational spectra for water in different zones adjacent to the hydrocarbon phase, we calculate the velocity autocorrelation function for the oxygen and hydrogen atoms of water and Fourier transform them to obtain the power spectrum, which can be interpreted as the density of states of different oscillators.

The velocity autocorrelation function (vacf) can be calculated for the oxygen and hydrogen atoms in water. We calculated both vacfs in all regions of each system in the laboratory frame, and the results are shown in Figure 5 for the water/TMP interface. These are representative of all five water/hydrocarbon

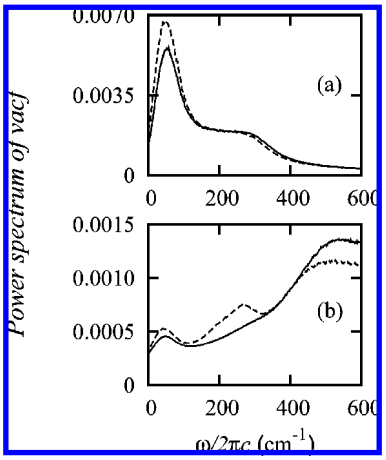

Figure 6. The power spectrum of the velocity autocorrelation function (vacf) for the interfacial (dashes) and bulk (solid lines) in the laboratory frame obtained for (a) the oxygen and (b) hydrogen atoms of water.

systems that we considered. The oxygen vacf (Figure 5a) shows a systematic trend going from the bulk to interfacial water. The first minimum corresponding to the back scattering of atoms is unchanged from the bulk to intermediate water, but it is shallower for interfacial water. At the interface, fewer hydrogen bonds are formed, but the hydrogen bonding is more efficient.[24] The former condition leads to faster rearrangement and is the likely reason for the observed trend. This scenario is corroborated by the hydrogen vacf, which also shows a deeper minimum for the bulk than for interfacial water. This trend in the velocity correlation function is identical to that observed in the vicinity of planar hydrophobic surfaces.[49] Comparison with a planar hydrophobic interface is best made in the intrinsic frame, and the velocity correlation functions are almost identical in both laboratory and intrinsic frames, thereby confirming this similarity with planar hydrophobic surfaces.

More insight into the local environment can be obtained through the power spectrum obtained by Fourier transforming the vacf. The power spectra so obtained are presented in Figure 6. The key features to be observed are peaks at frequencies around 50 (corresponding to O···O···O bending), 200 (corresponding to O···O stretching), and 500 cm^{-1} (corresponding to H-bond librational motion).[50] For the oxygen power spectrum, the first peak at 50 cm^{-1} corresponding to O···O···O bending becomes sharper with respect to the bulk at the interface, suggesting that the hydrogen-bonded network is stronger at the interface. This interpretation would be consistent with a strong hydrogen-bonded network at the interface. In the context of the water liquid/vapor interface, removing the effect of the diffusion of molecule pairs was found to lead to slower hydrogen-bond relaxation.[51] If interfacial water behaves in a similar fashion, the inter-oxygen angle is likely to be more rigid, and the sharper peak would be expected.

The librational mode can be interrogated with the power spectrum of the hydrogen atoms, which is presented in Figure 6. This spectrum shows a peak at about 50 cm^{-1} associated with the inter-oxygen angle bending, implying that the hydrogen atoms contribute to this mode. There is an enhancement in this peak over the bulk which further supports the picture of a stronger hydrogen-bonded network. It is intriguing that interfacial water exhibits a peak at 250 cm^{-1} which is absent in the bulk liquid. This would imply a higher density O···O bond-stretching mode than that of the bulk and is just another manifestation of the stronger hydrogen-bonded network at the interface. Since the intrinsic structure shows an enhanced density near the hydrocarbon surface which is broadened by capillary

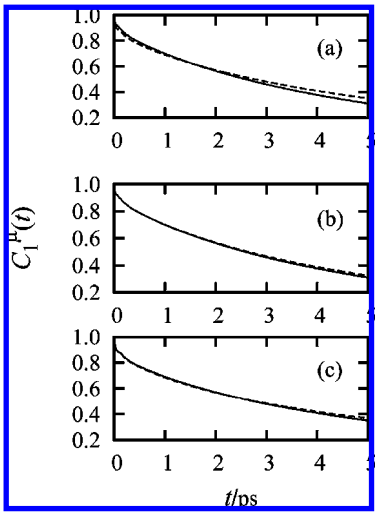

Figure 7. Dipole moment TCF for the $l = 1$ Legendre polynomial in the laboratory (solid line) and intrinsic frames (dashed line) for the (a) bulk, (b) intermediate, and (c) interfacial regions of the water/TMP system.

waves,[24] it would be natural to expect that these enhanced peaks arise from molecules that populate this region of enhanced density. The librational band at 500 cm^{-1} does not change its position, but its amplitude is reduced with respect to the bulk, suggesting a more flexible network, reflecting the fact that molecules near the hydrocarbon phase participate in fewer hydrogen bonds than those in bulk liquid. The overall picture of the interface is that of stronger hydrogen bonding and fewer hydrogen bonds per molecule at the interface. Consequently, the dynamics of hydrogen-bond formation and breaking should be slower at the interface, and this picture is supported by simulations.[52,53]

C. Rotational Motion. *1. Orientational Time Correlation Functions.* The interface provides a heterogeneous environment, and rotational dynamics are expected to be qualitatively different than that in the bulk.[54] To obtain insight into the effect of the interface on rotational dynamics, we studied orientational relaxation of the three principal axes of inertia of a water molecule, starting with dipole moment reorientation in different zones. We calculated the dipole moment orientational time correlation functions (TCFs) defined as

$$C_l^{\mu}(t) = \langle P_l[\hat{\mu}(0)\cdot\hat{\mu}(t)]\rangle \tag{6}$$

where $P_l(x)$ is the Legendre polynomial of order l and $\hat{\mu}(t)$ is the unit vector along the molecular dipole moment at time t. The time correlation function was calculated in a manner analogous to the mean squared displacement

$$C_l^{\mu}(\tau) = \frac{1}{n_t}\sum_{n=0}^{n_t}\frac{1}{N(n\Delta t, n\Delta t+\tau)} \sum_{i=1}^{N(n\Delta t, n\Delta t+\tau)} P_l[\hat{\mu}_i(n\Delta t+\tau)\cdot\hat{\mu}_i(n\Delta t)] \tag{7}$$

where $\hat{\mu}_i(t)$ is a unit vector along the dipole moment of molecule i at time t and $l = 1-5$.

The TCFs obtained for $l = 1$ for the water/TMP system are presented in Figure 7 for the laboratory and intrinsic frames. These TCFs are very similar to those obtained for all of the water/hydrocarbon systems that we considered. For the laboratory frame, the overall time dependence of the correlation

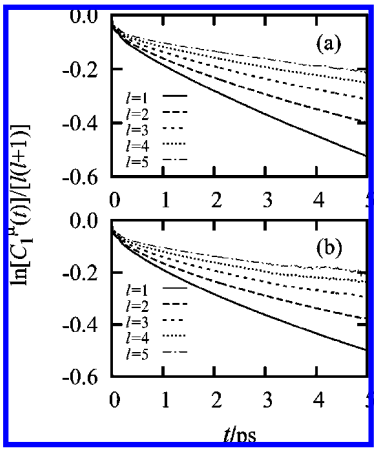

Figure 8. Dipole moment TCF of interfacial water; *l* dependence in the (a) laboratory and (b) intrinsic frames for the water/TMP system.

function is similar for each zone, although interfacial water exhibits a longer time decay, indicating slightly slower reorientation dynamics with respect to the bulk. The intermediate water layer exhibits a relaxation almost indistinguishable from bulk water. In the intrinsic frame, water dipole reorientation is slower than that in the laboratory frame. We also find that, just as for the laboratory frame, the dipole vector of interfacial water in the intrinsic frame reorients more slowly than that in the bulk.

In the case of translational motion, we were able to verify the existence of diffusive dynamics. A parallel question for orientational dynamics is, what is the nature of the long time orientational relaxation? One of the simplest descriptions of rotational dynamics is the Debye isotropic small-step diffusion model,[55] which predicts an exponential decay of the orientational correlation function $C_l(t) = \exp[-l(l+1)D_{rot}t]$, where D_{rot} is the isotropic rotational diffusion constant. If this relation holds, the scaled quantity $\ln[C_l(t)]/[l(l+1)]$ should be proportional to $-t$, and the slope should give us an *l*-independent rotational diffusion constant. In order to test this prediction, we calculated the correlation function for $l = 1-5$ and plotted the scaled TCF for interfacial water in Figure 8 for the laboratory and intrinsic frames.

As shown in Figure 7 for the case of $l = 1$, comparison of parts a and b of Figure 8 indicates that $C_l(t)$ relaxes slightly more slowly in the laboratory frame than in the intrinsic frame. This is expected since the orientational correlation function is a single-molecule quantity averaged over all molecules. As such, it will vary depending on the local environment, but within a selected region where all molecules sample a similar environment, a change in *l* should not affect the qualitative features of the dynamics.

In either frame, it is apparent that the scaled TCFs do not overlap for different values of *l* but decay more slowly as *l* increases, in disagreement with the isotropic rotational diffusion model. The time dependence of $\ln[C_l(t)]/[l(l+1)]$ is approximately linear at long times, with a slope that is different depending on the value of *l*. An *l*-dependent relaxation time clearly suggests the inapplicability of the simple Debye model for rotational relaxation. This difference between predicted and calculated time dependence could arise due to departure of real dynamics from the two assumptions of the Debye model, deviation from the small-angle jump[56−61] and anisotropy of rotational motion.[62]

We address the issue of large-angle jumps in rotational motion first. A simple model that invokes large-angle jumps is the Ivanov model,[56,57] which views rotational motion as consisting of angular jumps of the vector in question followed by a brief waiting period prior to the next jump. For SPC/E water, it was recently demonstrated that the O−H reorientation involved a large jump angle of about 60°, but instead of the O−H vector being stationary between jumps, it reoriented slowly through a rearrangement of the hydrogen-bond network during the waiting period.[29] After accounting for this additional relaxation time, an effective reorientation time scale was obtained for different *l*'s and found to be consistent with τ_l values from simulation. In view of this observation, it makes more sense to include the slow relaxation of the hydrogen-bond network, and we model the rotational motion of each principal axis in terms of the extended Ivanov model of Laage and Hynes.[29]

For the Ivanov model, the *l*th-order orientation correlation time, τ_l^h, is given by

$$\frac{1}{\tau_l^h} = \frac{1}{\tau_0^h}\left[1 - \frac{1}{2l+1}\frac{\sin[(l+1/2)\theta_0]}{\sin(\theta_0/2)}\right] \tag{8}$$

where θ_0 is the magnitude of the angular jump and τ_0^h is the average time between jumps. In the limit of small θ_0, the Ivanov model reduces to the Debye model, which predicts $\tau_1/\tau_2 = 3$. For large angular jumps on the order of $2\pi/(2l+1)$ or more, the Ivanov model predicts $\tau_1/\tau_2 = 1$. Thus, deviation of this ratio from 3 is indicative of angular jump motion, and the magnitude of the deviation corresponds to the magnitude of the angular jump.

In the extended Ivanov model,[29] the slow reorientation of the O···O vector of a pair of H-bonded molecules was found to be well described by the small-step diffusion model. The associated relaxation time τ_l^d is given by

$$\frac{1}{\tau_l^d} = \frac{l(l+1)}{\tau_0^d} \tag{9}$$

where τ_0^d is the inverse of the rotational diffusion constant, D_{rot}^{OO}, for motion of the vector connecting oxygen atoms of hydrogen-bonded pairs of molecules between hops. The observed rotational correlation time, τ_l, for a water molecule is then given by the following

$$\frac{1}{\tau_l} = \frac{1}{\tau_l^h} + \frac{1}{\tau_l^d} \tag{10}$$

As a first test of the rotational diffusion model, we calculate the *l* dependence of the dipole relaxation times, τ_l, for water molecules that populate the part of our simulation box designated as bulk water. These relaxation times can be measured by IR spectroscopy[63−65] as well as NMR[54,62,66] experiments. According to rotational diffusion models, the relaxation times, τ_l, correspond to the long time exponential decay of the correlation function and can be obtained by fitting the correlation function in this time regime for a given *l*. On the other hand, in some experiments, particularly NMR, the integral of the correlation function is used as a measure of the orientational correlation time. We therefore present a parallel analysis of rotational dynamics based on the two approaches for estimating the correlation times. The *l* dependence of the scaled correlation function, $\ln[C_l(t)]/[l(l+1)]$, for bulk water is qualitatively similar to that shown for interfacial water in Figure 8, and we do not present them here. The orientational relaxation times τ_l were calculated for $l = 1-5$ using the two approaches for obtaining them, and the values are presented in Table 3.

TABLE 3: *l* Dependence of the Dipole Orientational Correlation Time, τ_l (in ps), for the Water/TMP Interface[a]

	τ_1	τ_2	τ_3	τ_4	τ_5
(a) Exponential Fit					
simulation	4.96	2.28	1.59	1.28	1.08
predicted	4.98	2.23	1.61	1.32	1.04
(b) Integrated Time					
simulation	4.38	1.60	1.02	0.86	0.75
predicted	4.36	1.67	1.03	0.82	0.75

[a] The orientation correlation times are reported for the laboratory frame and were obtained using the two methods discussed in the text.

TABLE 4: Orientational Correlation Times, τ_l (in ps), for the Three Principal Axes of Interfacial Water and Different *l* in the Water/TMP System[a]

parameter	dipole	H−H	normal
τ_1	5.99	3.65	3.02
τ_2	2.80	2.56	2.41
τ_3	1.87	1.81	1.62
τ_4	1.46	1.54	1.42
τ_5	1.19	1.26	1.13
θ_0	84.5	123.6	141.8
τ_0^h	5.1	4.6	4.2
τ_0^d	41.9	41	36.8

[a] The results are reported for the laboratory frame and correspond to the best-fit parameters of the extended jump model.

On the basis of the time integral of the dipole reorientation correlation function, we estimate $\tau_1 = 4.38$ ps and $\tau_2 = 1.60$ ps. These time scales are consistent with published values[68] and verify the accuracy of our simulation. We obtained the ratio $\tau_1/\tau_2 = 2.7$, and this indicates departure from the isotropic small-angle diffusion models prediction of 3.0. Similar values of τ_1 and τ_2 were obtained for all of our interfacial systems. We estimate $\theta_0 = 49.8°$, $\tau_0^h = 1.1$ ps, and $\tau_0^d = 135.8$ ps by minimizing the sum of squared deviation between the simulated τ_l and values predicted by using eq 10. The predicted values of τ_l based on these parameters are presented in Table 3 and are in good agreement with our simulation. In view of the large value of τ_0^d, which enters eq 10 as its reciprocal, the effect of the slow network rearrangement on dipole vector reorientation should be very small due to its small magnitude. A simple Ivanov model description of dipole rotation should be sufficient if τ_l is estimated based on the time integral of the correlation function. Using a value of $\theta_0 = 46.9°$ in the Ivanov model, the ratio τ_1/τ_l for $l = 2-5$ is well described.

If the exponential decay times are used, as implicit in rotational diffusion models, the correlation times for different l values are larger than the time obtained from integrating the correlation function. From here on, only the exponential decay times are reported since they are the appropriate time scales for testing models. We obtained the extended model parameters by fitting the τ_l from simulations (as described in the previous paragraph) and found $\theta_0 = 81°$, $\tau_0^h = 3.7$ ps, and $\tau_0^d = 40.9$ ps. The agreement between the simulated and predicted τ_l values is again quite good. It should be noted that large-angle jumps were obtained irrespective of which method was used for estimating the correlation time, although the magnitude of the angular jump is dependent on the method used to obtain τ_l. The large value for θ_0 might be a consequence of fitting all of the τ_l values and further work is needed to verify the existence of such large jump angles. If we apply the Ivanov model instead of the extended Ivanov model, the jump angle is $\theta_0 = 72°$ based on the values of τ_1 and τ_2 only. However, on the basis of the minimization of the sum of squared deviations between τ_l values for $l = 1-5$ obtained from simulation and predicted by the Ivanov model, we obtained $\theta_0 = 54.9°$. The agreement between the Ivanov model and simulation data is satisfactory, although the extended Ivanov model is superior.

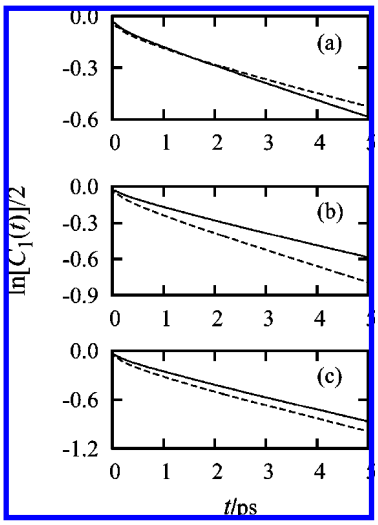

Figure 9. Orientational TCF for the $l = 1$ Legendre polynomial corresponding to bulk (solid line) and interfacial (dashed line) water for (a) the dipole moment unit vector, (b) the $\widehat{HH}$ unit vector, and (c) the vector normal to the molecular plane in the laboratory frame.

Turning to interfacial water, for the dipole vector, our data for τ_l for $l = 1-5$ is presented in Table 4 for the laboratory frame data only since the intrinsic frame shows similar behavior. The effect of the change in hydrocarbon was verified to be insignificant, and only the data for water/TMP is presented. On the basis of the τ_1 and τ_2 values, $\tau_1/\tau_2 = 2.14$ for the dipole vector at the interface, and the Debye model is clearly not applicable. Repeating the procedure adopted for bulk water, we obtained the parameters $\theta_0 = 84.5°$, $\tau_0^h = 5.1$ ps, and $\tau_0^d = 41.9$ ps. These values should be contrasted with the corresponding values for bulk water, $\theta_0 = 81°$, $\tau_0^h = 3.7$ ps, and $\tau_0^d = 40.9$ ps. Clearly, the rotational dynamics of the dipole vector are not significantly affected in the interfacial region compared to the bulk. The most significant difference appears to be an increase in the waiting time between hops from 3.7 to 5.1 ps, suggesting that rotation of the dipole vector is slightly slower at the interface. This of course is the trend observed when comparing the orientational correlation function for $l = 1$ for the dipole vector in Figure 9.

A second possible reason for the breakdown of the Debye model could be anisotropic rotation of the molecule. It is well-established that rotation of water is anisotropic about pairs of mutually perpendicular axes in the bulk.[62] Near the interface, reorientation of water might be more isotropic if low local density is the dominant factor affecting molecular reorientation. On the other hand, since diffusion perpendicular to the interface is slower than that in the bulk, perhaps rotational motion is also more anisotropic at the interface than that in the bulk, particularly in view of orientational preference of the O−H bond at hydrophobic interfaces. In order to gain insight into this issue, we compared the orientational TCFs for unit vectors along the three principal axes of water, the dipole moment vector ($\hat{u}$), the H−H vector ($\widehat{HH}$), and the normal ($\hat{n}$) to the plane of the molecule. For anisotropic rotation at the interface, these TCFs should lead to different relaxation times along different axes. The TCFs corresponding to the reorientation three principal axes of a water molecule for $l = 1$ are shown in Figure 9 for the water/TMP interface to illustrate anisotropy.

Our first observation is that the relaxation of the three principal axes of water is anisotropic in the bulk. We obtain τ_1

values of 4.96, 4.83, and 3.27 ps and τ_2 values of 2.28, 2.68, and 1.94 ps for the dipole, H−H, and $\hat{n}$ relaxation in bulk. These values are comparable to those reported previously for SPC/E water.[67,68] Rotation is therefore anisotropic for bulk water, although the relaxation times for two ($\hat{\mu}$ and $\widehat{HH}$) of the three vectors are similar and larger than the $\hat{n}$ relaxation times. This suggests that water reorientation is roughly isotropic for motion involving axes in the molecular plane and anisotropic normal to this plane. NMR measurements for the O−H relaxation (vector in the molecular plane) and $\hat{n}$ (normal to the molecular plane) support this picture of water reorientation.[62]

Just as for the dipole vector, we calculated orientational correlation times τ_l for $l = 1-5$ for $\widehat{HH}$ and $\hat{n}$ vectors. Fitting the l dependence of these times to the extended Ivanov model, we obtained $\theta_0 = 106.7$ and 101°, $\tau_0^{\mathrm{h}} = 5.8$ and 3.3 ps, and $\tau_0^{\mathrm{d}} = 34.5$ and 32.6 ps for the H−H and $\hat{n}$ principal axes, respectively. The jump angles for the H−H and $\hat{n}$ vector reorientations are comparable, suggesting that their reorientation might be correlated. However, the values of the waiting times between hops differ for these two vectors, making the correlation somewhat unclear. Compared to the dipole vector, the jump angles for the H−H and $\hat{n}$ vectors are much larger, although the waiting time for the $\hat{n}$ and dipole vectors are comparable. Clearly, a more detailed examination of rotational dynamics of the principal axes is needed to understand the mechanism of rotation of water molecules in bulk liquid.

The relaxation times for interfacial water along the $\widehat{HH}$ and $\hat{n}$ vectors are listed in Table 4. Compared to the bulk, at the interface, the dipole moment vector relaxes slower than that of the bulk, whereas the H−H and $\hat{n}$ vectors show a faster reorientation than that in the bulk. In particular, the H−H relaxation appears to be significantly faster at the interface. Since we were unable to find any published orientational correlation times for the water/hydrocarbon interface, comparison of this trend with other similar interfaces is not possible. The available data on the water/1,2-dichloroethane[22] and water/2-heptanone[23] interfaces indicate that dipole and $\widehat{HH}$ vector relaxations are slower for interfacial water. The reversal in trend for the H−H vector between the purely hydrophobic and the published data on polar organic molecular interfaces could be due to a different alignment of water molecules relative to the polar groups of the nonaqueous phase at these interfaces.

That water reorientation is anisotropic is fairly well-known, and various extensions of angular jump models have been formulated to account for this anisotropy.[69,70] Testing the applicability of those models is outside the scope of this work. However, it would still be useful to get some insight into the magnitude of angular jumps along the three principal axes of water, and we invoke the extended Ivanov model[29] for rotation about each axis, with the implicit assumption that motions along the principal axis are independent, thereby justifying its applicability.

The model parameters estimated based on τ_l for $l = 1-5$ are presented in Table 4 for the reorientation of the dipole, $\widehat{HH}$, and $\hat{n}$ principal axes. The set of jump angles for these axes changes from (81°,106.7°,101°) to (84.5°,123.6°,141.8°) upon going from bulk to interfacial water. There is a clear increase in anisotropy with respect to the bulk, but somewhat surprisingly, the jump angle for dipole vector reorientation is almost unchanged at the interface. The relaxation of each principal axis with the hydrogen-bonded network increases from (40.9,34.5, 32.6) to (41.9,41,36.8) ps, suggesting that the dipole vector sees a slower network reorientation than the $\widehat{HH}$ and $\hat{n}$ vectors at the interface. A change in waiting time from (3.7,5.8,3.3) ps in the bulk to (5.1,4.6,4.2) ps at the interface indicates that the dipole and $\hat{n}$ reorientation might be coupled since the waiting times for both of these axes increases at the interface. Rotation of the H−H vector is faster at the interface than that for the other axes presumably because of the reduction in the number of hydrogen bonds at the interface and is correlated with the observed trend in the correlation function for bulk and interfacial water shown in Figure 9.

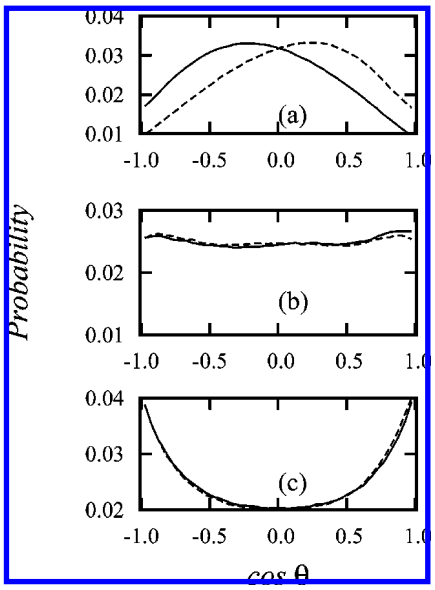

Figure 10. Probability of cos(θ) for molecules in the interfacial region, where θ is the angle between the $+z$ direction and (a) the unit dipole moment vector, (b) the H−H vector, and (c) the normal to the molecular plane of water for water molecules in the left (solid line) and right (dashed line) interfacial regions in the laboratory frame.

At the water/hydrocarbon interface, the strength of the hydrogen bonds increases, while their number decreases. These competing effects come closest to compensating in the case of the dipole, while they lead to faster relaxation than that in the bulk for the other two principal axes. This situation is expected to change if the polarity of the nonaqueous phase is increased by adding different polar groups. In view of the stronger hydrogen bonds at the interface, the hydrogen-bond dynamics is expected to be slower,[52] and our preliminary calculations support this expectation.

2. Dependence on the Initial Orientation. Structural studies of interfacial water at the water/hydrocarbon interface using second harmonic generation experiments and computer simulations reveal a preferential orientation of one O−H vector toward the hydrocarbon phase.[71−73] This is unlike bulk water where there is no average preferred orientation of the molecule. A detailed description of orientation is possible by specifying the two angular polar coordinates for a specified unit vector. With this two-angle representation, all accessible molecular orientations can be identified in computer simulations.[71,72,74−76] However, calculating well-averaged distributions and correlation functions for specific orientations in the two-angle description requires a lot more averaging and necessitates larger system sizes which are beyond the scope of this work. We therefore consider the orientation of a given unit vector with respect to the interfacial normal. Of course, the orientation of one molecular direction (O−H vector) provides insufficient information to completely specify the orientation of the water molecule, and we address this shortcoming by characterizing the molecular orientation in terms of the angles made by the three principal axes of the system with respect to the $+z$ direction for the interfacial region and compare it with the bulk.

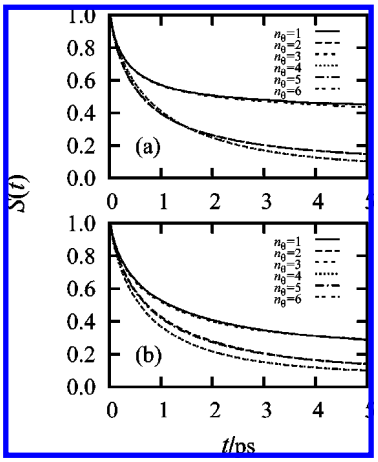

Figure 11. Survival TCF for the (a) dipole moment vector and (b) H−H vector of the water/TMP system for different initial orientations in the intrinsic frame.

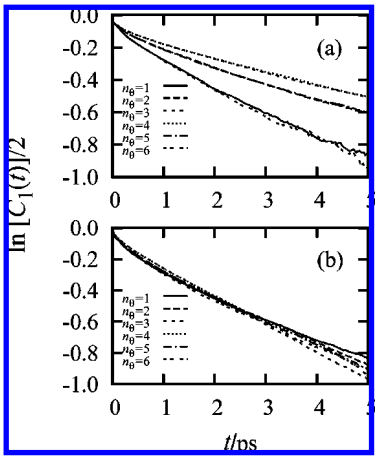

Figure 12. Initial orientation dependence of the $l = 1$ orientational TCF for the (a) dipole moment and (b) H−H vectors of interfacial water in the water/TMP system and for the intrinsic frame.

In previous work, we have studied the dipole orientation in terms of the second-order parameter profile $O_2(z) = \langle 3/2 \cos^2 \theta - 1/2 \rangle(z)$, where θ is the angle between the unit dipole vector and the z axis. A shortcoming of this order parameter is that $\cos(\pi - \theta) = -\cos \theta$, and information about the actual direction of the dipole vector with respect to the z axis is lost. A better order parameter to characterize orientations is $O_1(z) = \langle \cos \theta \rangle(z)$. Instead of calculating $O_1(z)$, we construct the distribution $P[\cos \theta]$ for the orientation of the three principal axes of water with respect to the $+z$ axis in the interfacial region and present the results in Figure 10.

The distribution for the molecular dipole vector is shown in Figure 10a. It should be noted that a molecule pointing the dipole vector toward the hydrocarbon phase on the left side of the aqueous phase would lead to a negative value for $\cos \theta$, whereas the same orientation at the right side of the aqueous phase would lead to an equal magnitude but a positive value for $\cos \theta$. In the presence of a preferred orientation toward the hydrocarbon phase, the peak position of the distribution should be shifted toward negative values for the left interface and toward positive values for the right interface, and this scenario is confirmed by the distribution constructed from our simulations. A second feature of interest is the asymmetry in the tail at $\cos \theta = 1$ or -1, which corresponds to more molecules pointing their dipole vector directly at the hydrocarbon phase than away from it.

The distribution of the H−H orientation is almost independent of $\cos \theta$, suggesting the lack of preferred orientation of this molecular axis at the interface. The distribution of orientations for the $\hat{n}$ vector reveals a strong preference for orienting toward the hydrocarbon phase. This enhanced density for the $\hat{n}$ orientation is associated with a reduction in density for the dipole vector orientation indicative of molecules aligned with the interfacial plane.

With the preferred orientation of the principal axes of interfacial water known, a natural query is, what are the implications of the orientational preference of molecules for their rotational dynamics? To gain insight into this, for each principal axis of a molecule, the angle made with the $+z$ axis, θ, is calculated, and the molecule is assigned to orientational subset n_θ, which contains molecules with angles in the range of $\{\theta_0, \theta_0 + \delta\theta_0\}$, where $\theta_0 = 30°(n_\theta - 1)$, with $n_\theta = 1-6$, and $\delta\theta_0 = 30°$. For each angular subset, the survival time correlation function is calculated and corresponds to the probability that a molecule in that angular subset stays in a selected region until time t, given that it was in the same region at time $t = 0$. Similarly, for each angular subset, we calculate the corresponding rotational TCF, which provides information on the dependence of rotational relaxation on the initial orientation of the molecule.

As shown earlier, dipole reorientation at the interface is slightly slower than that in the bulk, whereas H−H reorientation is faster. We present our results for the survival TCFs for orientational subsets $n_\theta = 1-6$ for these two principal axes in Figure 11. Since the intrinsic density profile reveals more structure than the laboratory frame profiles,[24] we present all TCFs in the intrinsic frame only. While not shown, for bulk water, these correlation functions are similar for all n_θ, and this is expected since there is no preferred orientation in bulk liquids.

For the dipole angular subsets, the significant trend in $S(t)$ is the clustering of the TCFs, one cluster containing $n_\theta = (1,6)$ and (2,5) and the other $n_\theta = (3,4)$. Molecules with their dipoles pointing toward the hydrocarbon surface in the subset $n_\theta = 1$ have two O−H covalent bonds facing the hydrocarbon phase. Such molecules serve as hydrogen-bond acceptors only and sacrifice two hydrogen bonds with other molecules. Molecules with $n_\theta = 6$ point their dipole 180° from the hydrocarbon surface, that is, away from the hydrocarbon surface. Clearly, such molecules at the interface will sacrifice two hydrogen bonds and serve as hydrogen-bond donors only. The dynamics of these molecules is expected to be driven by the need to increase their coordination to four hydrogen bonds from two, and on average, this leads to similar survival time probabilities for $n_\theta = 1$ and 6.

For $n_\theta = 2$ and 5, the dipole vector is oriented between 30 and 60° with respect to the z axis and includes molecules pointing one O−H covalent bond toward or away from the hydrocarbon phase. Such molecules can form up to three hydrogen bonds, and their contribution to the relaxation of the interfacial region is driven by rearrangement to form the extra hydrogen bond, thereby leading to similar $S(t)$ values for $n_\theta = 2$ and 5 but slower than $S(t)$ for $n_\theta = 1$. The decay of $S(t)$ for $n_\theta = 3$ and 4 water molecules is similar to the bulk, which could suggest these are involved in about four hydrogen bonds and are therefore more bulk-like than those for other n_θ's. The change in the time dependence of $S(t)$ with n_θ would suggest that a molecule with fewer hydrogen bonds will take the most time to form four hydrogen bonds before moving out of the interfacial region.

Turning to the H−H orientation, since the θ and $\pi - \theta$ orientations are equivalent, we should observe pairs of survival

time correlation functions, and this is the case indeed. For $n_\theta = 1$ and 6, the H−H vector is aligned with the z axis, and such molecules have their dipole vectors perpendicular to the z axis. Such dipole vectors belong to the angular set $n_\theta = 3$ or 4 and should survive in the interfacial zone for the longest time. Since motion along two principal axes could be independent, the correlation between the dipole and H−H reorientation might not be significant. In this scenario, the longer survival probability of the $n_\theta = 1$ subset could be due to the molecule's preference to rotate its H−H axis and reach a configuration more consistent with the dipole vector's preferred orientation. This rationalization would imply faster structural relaxation of the $n_\theta = 2$ subset followed by an even faster relaxation of the $n_\theta = 3$ subset.

We complement the initial orientation dependence of $S(t)$ with the $l = 1$ orientational TCFs for the dipole and H−H vectors in Figure 12. For the dipole moment vector, just as for the survival time correlation function, we find pairs of correlation functions corresponding to $n_\theta = (1,6)$, (2,5), and (3,4). For $n_\theta = (1,6)$, unlike $S(t)$, which has the slowest decay, $C_1(t)$ appears to have the fastest decay among all initial orientation subsets. This is perhaps not surprising since these water molecules have only two hydrogen bonds and the molecule would try to form the maximum number of hydrogen bonds, thereby leading to faster reorientation. The $n_\theta = (2,5)$ subset of molecules shows a slightly slower rotational dynamics, which is again consistent with the need to form more hydrogen bonds. The correlation function for $n_\theta = (3,4)$ shows a qualitatively similar relaxation to bulk water. In the case of H−H reorientation, variation between the orientational subsets is small, and no qualitative changes in rotational dynamics can be identified, in agreement with the distribution of orientations (Figure 10b). Longer residence times at the interface do not imply slower reorientation at the interface.

While it is tempting to interpret the orientational correlation times for different l values obtained for different initial orientation subsets in terms of the Debye or Ivanov or extended Ivanov model, any results are likely to be incorrect. As pointed out by Valiev and Ivanov,[57] a basic assumption in the derivation of the Debye or Ivanov model is that the probability of observing a rotation is independent of the initial orientation of the molecule. Our results for initial orientation dependence of the correlation functions clearly indicate a violation of this assumption. Furthermore, if a given orientation is preferred, perhaps rotations in space about that orientation are not symmetrically distributed about the preferred orientation. In this case, there might be a bias in the next diffusive step in angular space and would violate another assumption in deriving these rotational diffusion models. Clearly, if these assumptions are not satisfied, using the models to make predictions for the type of rotational diffusion would be incorrect, and we refrain from quantifying the correlation times and their modeling beyond qualitative features. Perhaps the large jump angles obtained upon application of the modified Ivanov model are indicative of the shortcomings of the model at interfaces.

IV. Hydrocarbon Dynamics

A. Translational Motion. We now turn to the interfacial dynamics of the hydrocarbon phase. In our studies of hydrocarbon interfacial structure, we found that hydrocarbon molecules stack at the interface,[24] leading to enhanced density adjacent to it. Certainly such stacking at the interface is expected to give rise to interesting dynamics.

As an indicator of translational mobility, we first calculate the survival TCFs for all zones, as described in Figure 1, in the laboratory frame. Our definition of the interfacial layer incorporates a very small number of molecules, leading to poor statistics. We therefore adjust the definition of the regions and relabel intermediate layer I3 and interfacial layer IF as the interfacial hydrocarbon phase. The survival TCFs for this interfacial region as well as those for the bulk are presented in Figure 13a for all hydrocarbons in series 1 and in Figure 13b for the series 2 hydrocarbons. For series 1, the survival TCF decays slowest for TMP followed by 2MP and P in the bulk as well as at the interface. Thus, it would appear that relaxation of the interfacial layer for series 1 hydrocarbons is dominated by molecular mass, and TMP, on account of its larger mass, should have the slowest relaxation. For series 2 hydrocarbons, the decay of $S(t)$ appears to be almost independent of the hydrocarbon phase, indicating that relaxation is not affected by branching for the same mass. On the basis of the behavior of all hydrocarbons, the picture that emerges is that molecular mass rather than branching dominates relaxation of the interfacial layer. A similar trend is seen for bulk and other intermediate hydrocarbon layers.

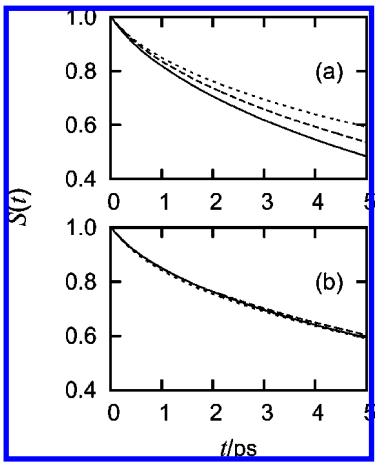

Figure 13. Survival TCF in the laboratory frame for the center of mass of interfacial hydrocarbons in (a) series 1 TMP (small dashes), 2MP (large dashes), and P (solid line) and (b) series 2 TMP (small dashes), 2MH (large dashes), and O (solid line).

To gain further insight into translational motion, we calculate the mean squared displacements and extract the diffusion constant parallel and perpendicular to the interface following the same procedure as that used for the aqueous phase. The estimates for the diffusion constants in the laboratory and intrinsic frames are listed in Table 5.

Compared to bulk, diffusion constants parallel to the interface appear to be larger for all interfacial hydrocarbons in both frames of reference. For motion perpendicular to the interface, the diffusion constants are much smaller and on the order of 0.04−0.11 Å^2/ps, indicating that diffusion perpendicular to the interface, at the interface, is almost independent of the hydrocarbon. The anisotropy in diffusion constant values in the plane and perpendicular to the interface is expected to decrease toward the region that we identify as the bulk.[21] The magnitude of D_{zz} for the hydrocarbon is smaller than that for interfacial water and is perhaps a consequence of the larger mass and the packing of the hydrocarbon molecules at the interface.[24]

B. Rotational Motion. In order to study the effect on the interface on reorientation of the hydrocarbon molecules, we calculate the orientational TCFs of the unit vector connecting the two terminal non-methyl sites on either end of the hydrocarbon chain. The direction of this vector was selected from the less branched (C_2) to the more branched (C_1) terminal.[24] The two questions that we wish to answer in this analysis are,

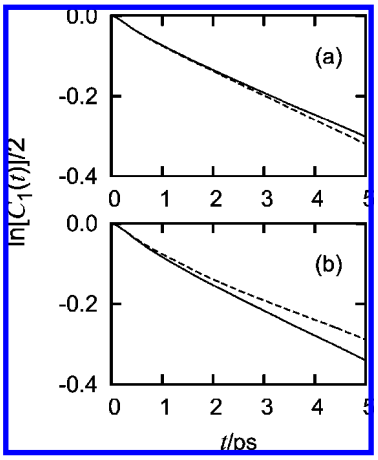

Figure 14. Orientational $l = 1$ TCF for the hydrocarbon C_1-C_2 vector for the water/TMP interface in the laboratory (solid line) and intrinsic (dashed line) frames for the (a) bulk and (b) interfacial hydrocarbon.

TABLE 5: In-Plane (D_{xy}) and Out-of-Plane (D_{zz}) Diffusion Constants for the Hydrocarbon Phase of the Five Water/Hydrocarbon Interfacial Systems[a]

D	P	2MP	TMP	2MH	O
D^{I}_{xy}	0.62	0.52	0.22	0.27	0.34
D^{L}_{xy}	0.61	0.47	0.32	0.33	0.37
D^{I}_{zz}	0.07	0.09	0.06	0.11	0.04
D^{L}_{zz}	0.05	0.06	0.06	0.06	0.06

[a] Values reported in units of Å^2/ps. Superscripts L and I correspond to the laboratory and intrinsic frames. The diffusion constants in the bulk phase are 0.41, 0.32, 0.18, 0.21, and 0.21 Å^2/ps for P, 2MP, TMP, 2MH, and O respectively.

TABLE 6: Orientational Correlation Times (in ps) for the Hydrocarbon C_1-C_2 Vector for the Five Interfacial Systems, τ_1 and τ_2, and Their Ratio τ_1/τ_2 in the Laboratory Frame

	P	2MP	TMP	2MH	O
			Bulk		
τ_1	3.46	4.87	9.13	17.77	20.58
τ_2	1.12	1.66	3.07	5.48	6.78
τ_1/τ_2	3.09	2.93	2.97	3.24	3.04
			Interface		
τ_1	5.64	7.56	9.88	34.02	37.62
τ_2	1.94	2.56	3.36	9.83	11.44
τ_1/τ_2	2.91	2.95	2.94	3.42	3.28

(a) how does rotational motion of the hydrocarbon differ from bulk and (b) what is the nature of rotational motion (small step diffusive vs jump)?

For insight into the reorientation dynamics, we calculate the $l = 1-5$ orientational TCFs for the C_1-C_2 vector for all series 1 and 2 hydrocarbons and present our results for the $l = 1$ correlation function for the water/TMP interface in Figure 14 (see also Table 6). For the bulk hydrocarbon phase, both the laboratory and intrinsic frame correlation functions are comparable. This indicates that our definition of the bulk phase is far enough from the water surface for the effect of the interface on rotational dynamics to be minimal. In the case of the interfacial hydrocarbon, the TCF is more influenced by the frame of reference, with the intrinsic frame being associated with a slower reorientation. Since the hydrocarbon intrinsic position was obtained with respect to a planar reference water surface, the picture of hydrocarbon reorientation that emerges is that of slow reorientation of molecules near the water surface. Since capillary fluctuations of the water surface will change the positions of the hydrocarbon molecules, the reorientation of these molecules is also expected to be faster. This should be contrasted with the small effect that we observed for interfacial water presumably due to the ability of water molecules to form hydrogen bonds unlike the hydrocarbon molecules. In view of this frame dependence, it makes more sense to study rotational dynamics in the intrinsic frame. This variation between bulk and interfacial hydrocarbon dynamics in the laboratory and intrinsic frames was also seen for the aqueous interface.

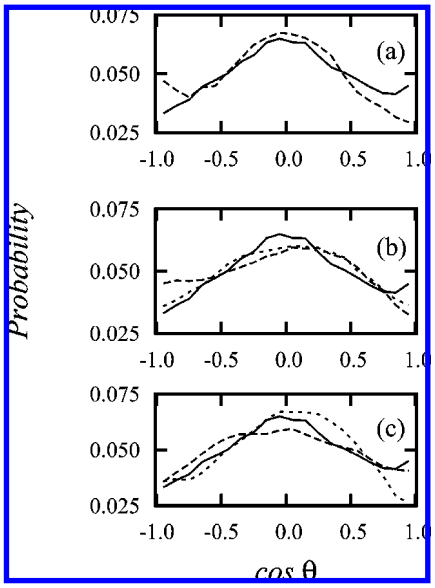

Figure 15. Probability of cos θ for interfacial molecules, where θ is the angle between the $+z$ axis and the unit C_1-C_2 vector of the hydrocarbon in the laboratory frame for the (a) TMP distribution at the left (solid line) and right (large dashes) interfaces, (b) series 1 TMP (solid line), 2MP (large dashes), and P (small dashes), and (c) series 2 TMP (solid line), 2MH (large dashes), and O (small dashes) for the left interface only.

Turning to the type of rotational motion, we estimate the orientational relaxation times τ_1 and τ_2 from the $l = 1$ and 2 orientational TCFs. Their ratio is indicative of the type of rotational dynamics, and we present the values for all three quantities in Table 6 for all interfacial systems. For any given system, on the basis of τ_1 and τ_2 values, interfacial hydrocarbons reorient more slowly than in the bulk, which is consistent with our qualitative observation from Figure 14. For series 1 hydrocarbons, the τ_l values increase from P to TMP in the bulk as well as the interface. Since the chain length is similar for all hydrocarbon molecules in this group, an increase in branching is associated with an increase in mass, and this appears to be the dominant factor. For hydrocarbons in series 2, the increased extent of branching appears to decrease τ_1 from 37.62 ps for O (no branching) at the interface to 9.88 ps for TMP (most branching). This change in rotation correlation times is likely to be an effect of molecular arrangement at the interface. Turning to the mechanism of reorientation at the interface, the ratio τ_1/τ_2 changes from less than 3.0 for series 1 hydrocarbons to more than 3.0 for the longer hydrocarbons in series 2. A ratio larger than 3.0 is indicative of restricted rotational motion and indicates that the rotation of the longer hydrocarbons is more restricted. We note that torsional and rotational motions of the hydrocarbon molecules are coupled, and we do not expect models developed for rigid-molecule reorientation to be entirely applicable.

If rotational motion is indeed restricted, it would be useful to study how the arrangement of molecules at the interface leads to such restricted motion. Analogous to the aqueous phase, we construct the distribution $P[\cos\theta]$, where θ is the angle made

by the C_1-C_2 vector with respect to the $+z$ axis and present our results in Figure 15.

A key feature of all distributions is the peak at $\cos\theta \approx 0$ indicative of orientation perpendicular to the $+z$ axis. A molecule with this orientation is in the plane of the interface, and the collection of such molecules corresponds to a stacked arrangement at the interface. Of course, stacking is limited by the interfacial area available to the molecules, and deviations from such orientation are expected after a certain number of molecules adopt this orientation. For the water/TMP interface (Figure 15a), there is a slight increase in the probability of finding molecules with their less branched end pointing toward the aqueous phase. This orientation would lead to low steric hindrance for the stacked molecules, and such molecules probably fill up the empty interfacial area left after stacking.

For series 1 hydrocarbons, the decrease in branching from TMP to P allows more molecules to stack at the interface, and this leads to a broader distribution of orientations. However, the position of the peak shifts to slightly larger values of $\cos\theta$, indicating orientation at an angle with respect to the hydrocarbon surface. The second preferred orientation for both of the branched molecules is aligning the 2-methyl side parallel to the $+z$ axis, which shows up as an enhancement at large $\cos\theta$ for TMP and large negative values for 2MP. Pentane, by virtue of its straight chain, does not exhibit a significant orientation perpendicular to the interface possibly due to more molecules stacking at the interface. For series 2, 2MH has a broader distribution of orientations while being qualitatively similar to TMP presumably due to an increase in chain length. Just as for 2MP, 2MH shows a small preference for aligning the 2-methyl side with the $+z$ axis. Octane being the longest hydrocarbon in the series shows a preference for alignment at an angle with the interface instead of being completely in the plane of the interface. Molecules showing a broader distribution of orientations or a peak shifted from zero are oriented at an angle with respect to the interface, and the rotational motion of such molecules is expected to be restricted by adjacent molecules; this might be the reason why $\tau_1/\tau_2 > 3$ for the longer molecules in series 2.

With an orientational preference at the interface for the hydrocarbon, it is possible that molecules with different initial orientations might reorient in different ways, just as for the aqueous interface. In order to test this possibility, interfacial molecules are partitioned into angular sets $n_\theta = 1-4$ with angles in the range of θ_0 and $\theta_0 + \delta\theta_0$, where $\theta_0 = (n_\theta - 1)45°$ and $\delta\theta_0 = 45°$. The angular range was increased to 45 from 30° for water to improve the statistics since there are fewer hydrocarbon molecules at the interface. The survival time and orientation time correlation functions for each angular subset n_θ are presented in Figure 16 for the water/TMP interface in the laboratory frame to illustrate the initial orientation dependence.

Just as for water, we find that the hydrocarbon survival and orientation time correlation functions occur in pairs for angular subsets oriented symmetrically with respect to the $+z$ axis. Molecules in the angular subset $n_\theta = 1$ and 4 survive in the interfacial region for the longest time, although their reorientation is the fastest. On the other hand, molecules in the angular subset $n_\theta = 2$ and 4 survive in the interfacial region for a shorter time than those in $n_\theta = 1$, but their orientation time correlation functions exhibit a longer time decay. This inverse correlation between the survival and rotation time scales is similar to the aqueous interface and indicates that molecules with the preferred orientation at the interface rotate the slowest, although their rotation is coupled to relaxation of the interfacial layer and they tend to move out of this layer faster than molecules with other orientations.

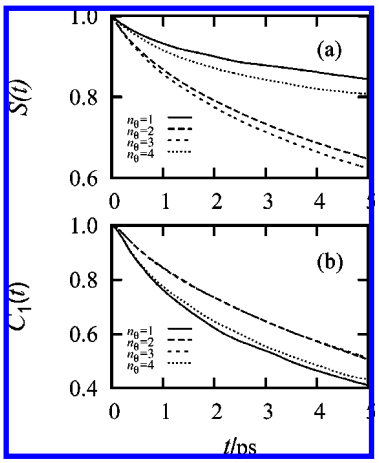

Figure 16. Initial orientation dependence of (a) the survival TCF, $S(t)$, and (b) the $l = 1$ orientational TCF for the hydrocarbon C_1-C_2 vector for the water/TMP system in the laboratory frame.

V. Summary

Single-molecule relaxation is studied for the water and hydrocarbon components of five water/hydrocarbon interfaces using molecular dynamics simulations with the objective of identifying the effect of hydrocarbon branching on the dynamics. Each liquid phase is partitioned into regions of 5 Å width, and the effect of the presence of the interface on regions near and away from the interface is studied.

Relaxation of the interfacial layer was studied using the survival TCF of the molecular center of mass and indicates that molecules at the interface stay in the interfacial region for a longer time than those in the corresponding bulk phase of the system. Translational motion was further quantified in terms of the diffusion constants parallel and perpendicular to the interface since the diffusion tensor is diagonal in this frame. In-plane diffusion constants were calculated using the formalism of Liu et al.,[26] while diffusion constants perpendicular to the interface were approximately obtained from the difference in the total and in-plane diffusion constants. Further work is necessary for a quantitative analysis of diffusion perpendicular to the interface and the effect of interfacial fluctuations. Motion perpendicular to the interface was found to be slower, whereas diffusion constants for motion in the plane of the interface was found to be faster than that in bulk. Such translational dynamics is a consequence of the geometrical confinement as well as density variation at the interface.

Turning to the rotational motion of water, the orientational TCFs were calculated for the three principal axes. Rotational motion was found to be slower for the dipole vector and faster for the H−H and normal to the molecule plane vectors, and this anisotropy increased from the bulk toward the interface. The l dependence of the corresponding correlation times were analyzed successfully in terms of the modified Ivanov model of Laage and Hynes.[29] It would be useful to perform a detailed analysis of rotational dynamics for interfacial water in order to make a connection of the jump angles obtained from an analysis of the l-dependent rotation correlation times with the actual jump motions, and this will be considered in future work. Similar qualitative features were observed for the interfacial hydrocarbon phase.

At the interface, molecular orientation is anisotropic, with a distribution of possible alignments with respect to the surface normal for water as well as for the hydrocarbon molecules. Water molecules tend to align one O−H covalent bond toward the hydrocarbon phase, whereas the hydrocarbon molecules stack up in the plane of the interface. The consequence of such preferred orientations on dynamics was studied in terms of the survival and rotation time correlation functions, and a starting orientation dependence was observed. Molecules with the preferred orientation tend to rotate more slowly than those in the bulk, although they tend to stay in the interfacial region for the shortest time, thereby implying an inverse relation between rotational and translational time scales. In view of these observations, rotation diffusion models cannot be applied in the interfacial region since they assume isotropic orientations and independence from initial orientation. Clearly, new models need to be developed for a quantitative description of rotational motion at the interface.

While this work has focused on single-molecule properties like translational diffusion and orientational relaxation, these results have implications for collective motion of water molecules at the interface. In particular, a study of the dynamics of the hydrogen-bonded network or correlations between the density or height fluctuations due to capillary waves at the interface would be very useful, given the insight from single-molecule dynamics. This is another issue that will be addressed in subsequent work.

A primary objective of this work was to identify the effect of hydrocarbon branching on dynamics. We do not find a significant change in dynamical behavior of the aqueous interfacial region with changes in the hydrocarbon phase. This, at first, surprising observation is less puzzling if we consider that the aqueous phase shows small variation in the density and intrinsic density profiles upon changing the hydrocarbon phase.[24] If structure and dynamics are related, then for the five hydrocarbons considered, dynamics should not be significantly affected. Clearly, the aqueous phase tries to maintain its hydrogen-bonded structure and is not significantly perturbed by the free hydrocarbon molecules. The interfacial hydrocarbon, on the other hand, shows large variation in the dynamics, although this does not affect the water phase. Perhaps studying hydrocarbons with much longer chains or branched structures could lead to more significant changes in the interfacial properties, and it would be interesting to test this possibility.

A secondary aim of this work was to identify the effect of capillary waves on the dynamics. Since this analysis requires mapping of the molecules of one liquid to the surface sites of the other liquid, dynamics are accelerated due to the coupling to the dynamics of the surface sites. This speed up was found in the survival time correlation functions as well as the diffusion constants. For rotational motion, the decay of the orientational TCFs was found to be slightly slower in the intrinsic than that in the laboratory frame, implying that capillary wave fluctuations of the interface do not significantly affect rotational motion.

Acknowledgment. This work was supported by the DOE Grant DE-FG03-0ZER15376 and by the NSF Grant CHE 0608640.

References and Notes

(1) Gregory, R. B., Ed. *Protein−Solvent Interactions*; Marcel Dekker, Inc.: New York, 1995.
(2) Pal, S. K.; Peon, J.; Bagchi, B.; Zewail, A. H. *J. Phys. Chem. B* **2002**, *106*, 12376.
(3) Bizzarri, A. R.; Cannistraro, S. *J. Phys. Chem. B* **2002**, *106*, 6617.
(4) Lopez, C. F.; Nielsen, S. O.; Klein, M. L.; Moore, P. B. *J. Phys. Chem. B* **2004**, *108*, 6603.
(5) Bhide, S. Y.; Berkowitz, M. L. *J. Chem. Phys.* **2005**, *123*, 224702.
(6) Faeder, J.; Ladanyi, B. M. *J. Phys. Chem. B* **2000**, *104*, 1033.
(7) Harpham, M. R.; Ladanyi, B. M.; Levinger, N. E. *J. Phys. Chem. B* **2005**, *109*, 16891.
(8) Harpham, M. R.; Ladanyi, B. M.; Levinger, N. E.; Herwig, K. W. *J. Chem. Phys.* **2004**, *121*, 7855.
(9) Abel, S.; Sterpone, S.; Bandyopadhyay, S.; Marchi, M. *J. Phys. Chem. B* **2004**, *108*, 19458.
(10) Sterpone, F.; Marchetti, G.; Pierleoni, C.; Marchi, M. *J. Phys. Chem. B* **2006**, *110*, 11504.
(11) Benjamin, I. *Annu. Rev. Phys. Chem.* **1997**, *48*, 407.
(12) Kazarinov, V. E. *The Interface Structure and Electrochemical Processes at the Boundary between Two Immiscible Liquids*; Springer : Berlin, 1987.
(13) Morrow, N. *Interfacial Phenomena in Petroleum Recovery*; Dekker: New York, 1990.
(14) Martins, L. R.; Skaf, M. S.; Ladanyi, B. M. *J. Phys. Chem. B* **2004**, *108*, 19687.
(15) Hartnig, C.; Witschel, W.; Spohr, E.; Gallo, P.; Ricci, M. A.; Rovere, M. *J. Mol. Liq.* **2000**, *85*, 127.
(16) Gallo, P.; Rovere, M. *J. Phys.: Condens. Matter* **2003**, *15*, 7625.
(17) Rovere, M.; Gallo, P. *Eur. Phys. J. E* **2003**, *12*, 77.
(18) Thompson, H.; Soper, A. K.; Ricci, M. A.; Bruni, F.; Skipper, N. T. *J. Phys. Chem. B* **2007**, *111*, 5610.
(19) Michael, D.; Benjamin, I. *J. Electroanal. Chem.* **1998**, *450*, 335.
(20) Riedleder, A. J.; Kentish, S. E.; Perera, J. M.; Stevens, G. W. *Solvent Extr. Ion Exch.* **2007**, *24*, 41.
(21) Michael, D.; Benjamin, I. *J. Phys. Chem.* **1995**, *99*, 1530.
(22) Benjamin, I. *J. Chem. Phys.* **1992**, *97*, 1432.
(23) Fernandes, P. A.; Cordeiro, M. N. D. S.; Gomes, J. A. N. F. *J. Phys. Chem. B* **1999**, *103*, 6290.
(24) Chowdhary, J.; Ladanyi, B. M. *J. Phys. Chem. B* **2006**, *110*, 15442.
(25) Klafter, J.; Zumofen, G.; Blumen, A. *Chem. Phys.* **1993**, *177*, 821.
(26) Liu, P.; Harder, E.; Berne, B. J. *J. Phys. Chem. B* **2004**, *108*, 6595.
(27) Wang, C. C.; Pecora, W. *J. Chem. Phys.* **1980**, *72*, 5333.
(28) Lipari, G.; Szabo, A. *J. Chem. Phys.* **1981**, *75*, 2971.
(29) Laage, D.; Hynes, J. T. *Science* **2006**, *311*, 832.
(30) Rowlinson, J. S.; Widom, B. *Molecular Theory of Capillarity*; Clarendon Press: Oxford, U.K., 1982.
(31) Buff, F.; Lovett, R.; Stillinger, F. *Phys. Rev. Lett.* **1965**, *15*, 621.
(32) Percus, J. R. In *Fluid Interfacial Phenomena*; Croxton, C. A., Ed.; John Wiley:New York, 1986, pp 1−44.
(33) Berendsen, H. J. C.; Grigera, J. R.; Straatsma, T. P. *J. Phys. Chem.* **1987**, *91*, 6269.
(34) Jorgensen, W. L.; Madura, J. D.; Swenson, C. J. *J. Am Chem. Soc.* **1984**, *106*, 6638.
(35) Allen, W.; Rowley, R. L. *J. Chem. Phys.* **1997**, *106*, 10273.
(36) Wolf, D.; Keblinski, P.; Phillpot, S. R.; Eggebrecht, J. *J. Chem. Phys.* **1999**, *110*, 8254.
(37) Demontis, P.; Spanu, S.; Suffritti, G. B. *J. Chem. Phys.* **2001**, *114*, 7980.
(38) Zahn, D.; Schilling, B.; Kast, S. M. *J. Phys. Chem. B* **2002**, *106*, 10725.
(39) Sepliarsky, M.; Stachiotti, M. G.; Migoni, R. L. *Phys. Rev. B* **2005**, *72*, 014110.
(40) Ewald. P. *Ann. Phys.* **1921**, *64*, 253.
(41) Allen, M. P.; Tildesley, D. J. *Computer Simulation of Liquids*; Oxford University Press: New York, 1989.
(42) Fennell, C. J.; Gezelter, J. D. *J. Chem. Phys.* **2006**, *124*, 234104.
(43) Berendsen, H. J. C.; Postma, J. P. M.; van Gunsteren, W. F.; DiNola, A.; Haak, J. R. *J. Chem. Phys.* **1984**, *81*, 3684.
(44) Rochhi, C.; Bizzarri, A. R.; Cannistraro, S. *Phys. Rev. E* **1998**, *57*, 3315.
(45) Dastidar, S. G.; Mukhopadhyay, C. *Phys. Rev. E* **2004**, *70*, 061901.
(46) Winkler, R. G.; Schmid, R. H.; Gerstmair, A.; Reineker, P. *J. Chem. Phys.* **1996**, *104*, 8103.
(47) Peters, E. A. J. F.; Barenbrug, Th. M. A. O. M. *Phys. Rev. E* **2002**, *66*, 056701.
(48) Sega, M.; Vallauri, R.; Melchionna, S. *Phys. Rev. E* **2005**, *72*, 041201.
(49) Lee, S. H.; Rossky, P. J. *J. Chem. Phys.* **1994**, *100*, 3334.
(50) Ohmine, I.; Saito, S. *Acc. Chem. Res.* **1999**, *32*, 741.
(51) Liu, P.; Harder, E.; Berne, B. J. *J. Phys. Chem. B* **2005**, *109*, 2949.
(52) Benjamin, I. *J. Phys. Chem. B* **2005**, *109*, 13711.
(53) Chowdhary, J.; Ladanyi, B. M. Unpublished results.
(54) Halle, B.; Wennerstrom, H. *J. Chem. Phys.* **1981**, *75*, 1928.
(55) Berne, B. J.; Pecora, R. *Dynamic Light Scattering: With Applications to Chemistry, Biology and Physics*; Wiley: New York, 1976.
(56) Ivanov, E. N. *Sov. Phys. JETP* **1964**, *18*, 1041.
(57) Valiev, K. A.; Ivanov, E. N. *Sov. Phys. Usp.* **1973**, *16*, 1.
(58) Gelin, M. F.; Kosov, D. S. *J. Chem. Phys.* **2006**, *124*, 144514.

(59) Kivelson, D.; Keyes, T. *J. Chem. Phys.* **1972**, *57*, 4599.
(60) Fixman, M.; Rider, K. *J. Chem. Phys.* **1969**, *51*, 2425.
(61) Gordon, R. G. *J. Chem. Phys.* **1966**, *44*, 1830.
(62) Ropp, J.; Lawrence, C.; Farrar, T. C.; Skinner, J. L. *J. Am. Chem. Soc.* **2001**, *123*, 8047.
(63) Lawrence, C. P.; Skinner, J. L. *J. Chem. Phys.* **2003**, *118*, 264.
(64) Tan, H. S.; Piletic, I. R.; Fayer, M. D. *J. Chem. Phys.* **2005**, *122*, 174501.
(65) Fecko, C. J.; Loparo, J. J.; Roberts, S. T.; Tokmakoff, A. *J. Chem. Phys.* **2005**, *122*, 054506.
(66) Rothschild, W. G. *Dynamics of Molecular Liquids*; Wiley: New York, 1984.
(67) Svishchev, I. M.; Kusalik, P. G. *J. Phys. Chem.* **1994**, *98*, 728.
(68) van der Spoel, D.; van Maaren, P. J.; Berendsen, H. J. C. *J. Chem. Phys.* **1998**, *108*, 10220.
(69) Diezemann, G.; Sillescu, H. *J. Chem. Phys.* **1999**, *111*, 1126.
(70) Alessi, L.; Andreozzi, L.; Faetti, M.; Leporini, D. *J. Chem. Phys.* **2001**, *114*, 3631.
(71) Jedlovszky, P.; Vincze, A.; Horvai. G. *J. Mol. Liq.* **2004**, *109*, 99.
(72) Jedlovszky, P.; Vincze, A.; Horvai. G. *Phys. Chem. Chem. Phys.* **2004**, *6*, 1874.
(73) Brown, M. G.; Walker, D. S.; Raymond, E. A.; Richmond, G. L. *J. Phys. Chem. B* **2002**, *107*, 237.
(74) Partay, L.; Jedlovszky, P.; Horvai, G. *J. Phys. Chem. B* **2005**, *109*, 12014.
(75) Partay, L.; Jedlovszky, P.; Jancso, G. *Chem. Phys. Lett.* **2006**, *420*, 367.
(76) Hore, D. K.; Walker, D. S.; MacKinnon, L.; Richmond, G. L. *J. Phys. Chem. C* **2007**, *111*, 8832.